Available online at www.sciencedirect.com

ScienceDirect

Procedia CIRP 74 (2018) 511–517

www.elsevier.com/locate/procedia

10th CIRP Conference on Photonic Technologies [LANE 2018]

Determination of sensitivity and thermal efficiency in laser assisted metal-plastic joining by numerical simulation

Klaus Schricker[a,]*, Jean Pierre Bergmann[a]

[a]*Technische Universität Ilmenau, Department of Mechanical Engineering, Production Technology Group*

* Corresponding author. Tel.: +49-3677-69-3808 ; fax: +49-3677-69-1660. *E-mail address:* info.fertigungstechnik@tu-ilmenau.de

Abstract

Laser-assisted joining of plastics and metals requires the formation of a melting layer in the thermoplastic material, which enables the wetting and the penetration of the metal surface. In this paper, a generally valid description of the melting layer is given based on material-specific temperatures and numerical simulation. Furthermore, the sensitivity of the melting layer to process parameters, material properties and geometrical parameters is provided. Based on these results, the thermal efficiency of the process was examined depending the major factors metal thickness and absorbed laser beam power.

Peer-review under responsibility of the Bayerisches Laserzentrum GmbH.

Keywords: laser welding; metal-plastic hybrid; hybrid joints; LAMP; thermal joining; thermal degradation; numerical simulation

1. Introduction and state of the art

The use of multi-material design is one of the leading issues in engineering constructions regarding functional integration and cost-efficient products. In this field, the combination of metals and plastics is a promising approach to meet the requirements combining materials with opposed properties. Especially in case of industrial applications for white goods industry, aluminum and steel are widely used metals. On side of the plastic materials, large-scale production relies mainly on thermoplastic materials, manufactured by injection moulding or extrusion processes. Thereby, joining technology is a key parameter in creating those multi-material designs at a cost-efficient level. Especially in case of metal plastics joints, nowadays mostly adhesives or joining elements are used, with some restrictions, e. g. curing times or tension peaks.

However, thermal joining offers great advantageous over these competitive processes by creating a direct connection between both materials and avoiding the named disadvantageous of the currently used joining processes.

In thermal joining, both materials are in contact at the boundary layer. The metal sheet is warmed up and the heat is conducted through the metal sheet into the plastic material. Due to the heat transfer, the thermoplastic material forms a melting layer of liquified material at the boundary layer [1]. This melting layer must provide enough molten material for wetting the metal surface and penetrating the surface structures, to form a solid joint after solidification.

This process can be carried out by several energy sources, e. g. laser radiation [2] or induction heating [3]. The advantageous of a laser-based joining process are the geometrically independent and contactless energy input as well as the possibility to create tight and areal joints [4].

Hybrid joints are widely characterized regarding the interaction between mechanical properties, surface preparation and process parameters [5-6] as well as for behavior under temperature load, weathering and corrosive media [7-8]. Further investigations were carried out on joining mechanism for different materials and surface preparations [1-2, 9].

However, the melting layer as enabler for forming a joint between both materials is superficially investigated yet and not finally correlated to the temperature distribution within

2212-8271 © 2018 The Authors. Published by Elsevier Ltd. This is an open access article under the CC BY-NC-ND license (https://creativecommons.org/licenses/by-nc-nd/4.0/)
Peer-review under responsibility of the Bayerisches Laserzentrum GmbH.
10.1016/j.procir.2018.08.133

both joining partners. A more detailed view on the melting interval and beyond the mainly used peak melting temperature could describe occurring effects, e. g. different thermoplastic morphologies of a completely and a partially molten zone within the melting layer as well as the appearance of an adjoined heat affected zone [7, 10]. This requires information about the material properties as well as the temperature distribution. The material data can be provided by thermal analysis and the temperature distribution can be determined by numerical simulation of the laser-based joining process [10-14]. So far, numerical simulations were mainly used to gain information about the temperature-time profile within the interface and to confine process parameters. However, several simplifications were made on temperature dependent material data [11-13], the neglection of the phase transition within the thermoplastic material [11-14] and the use of a melting point instead of a melting interval on side of the thermoplastic material [11-12].

In conclusion, the melting layer represents the key parameter for forming a joint between thermoplastic materials and metals but is not sufficiently described yet. A description could be given by the temperature distribution between both joining partners by considering the phase-transition and the melting interval. Based on these information, the interaction between material properties and process parameters regarding the geometry of the melting layer can be given. On this basis, the impact of the significant process parameters on thermal efficiency can be provided towards the realization of economically valuable processes.

2. Experimental setup

The experiments were carried out using a diode laser (Laserline LDM 3000) with a mean wavelength of 980 nm, a focal diameter d_L of 5.3 mm and a maximum beam power of 3 kW. A three-axis processing table was used for manufacturing the hybrid joints (figure 1a). In terms of fundamental research, spot joints were manufactured in heat conduction joining and based on an overlap configuration of 100 mm length and 75 mm width. Joining times were used from 1 s up to 10 s. The distance between clamping jaws was set to 50 mm to limit the effect on temperature distribution.

As metal joining partner, aluminum EN AW 6082 (t_M = 1.5 mm) was used as well as steel 1.4301 (comparable to AISI304 or X5CrNi18-10, t_M = 1 mm). The investigations were carried out mainly on two surface conditions: As delivered and laser-manufactured grooves with a width of 25 µm and a depth of 30 µm by a pulsed fibre laser (Rofin PowerLine F20, see also [7]). On side of the thermoplastics, polyamide 6 (PA 6), polyamide 6.6 (PA 6.6) as well as polypropylene (PP) were used. A thickness of 5 mm was chosen to ensure the presence of semi-infinite domain as known from heat transfer problems. Therefore, the bottom of the plastic sheet is at no time affected by the heat input at the top during the process and heat accumulation is avoided within the overlap joint (figure 1b).

Based on the joining process, a melting layer is formed within the plastic material and evaluated regarding its diameter and thickness (figure 1b). This area depends on the temperature distribution within both joining partners and shows different morphological zones. In order to include these zones depending on material specific temperatures, three temperatures are defined: T_{im} [K] as begin respectively T_{em} [K] as end of the thermoplastic material's melting interval and T_d [K] as degradation temperature when decomposition occurs. The necessary material data were examined by differential scanning calorimetry (heating rate: 10 K·min^{-1}) as well as thermogravimetric analysis (heating rate: 20 K·min^{-1}).

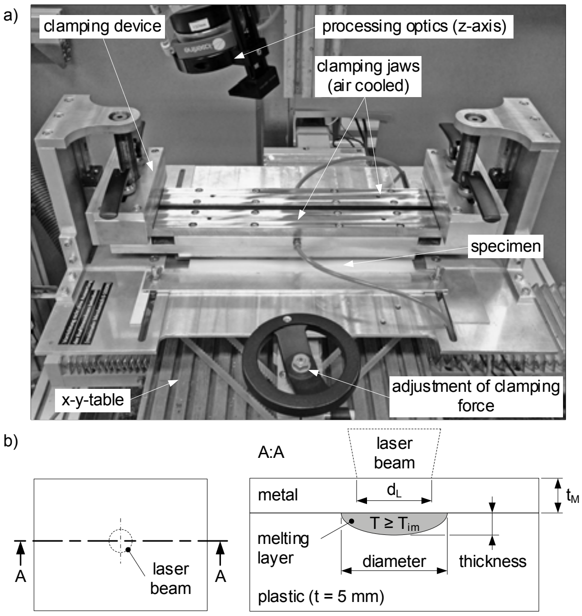

Fig. 1. a) experimental setup and b) overlap configuration

3. Numerical simulation

3.1. Model assumptions and geometry

A thermal model was set up for describing the temperature distribution in both joining partners and evaluating the melting layer within the thermoplastic material. Based on the simplifications (spot joints, semi-infinite body), a rotationally symmetric, transient 2D geometry was used for numerical simulation in Comsol Multiphysics 5.2a.

The transient heat transfer within the joining partners is based on the heat equation (1) with heat flow $\dot{Q}$ [W], density ρ [kg·m^{-3}], heat capacity c_p [J·kg^{-1}·K^{-1}] and thermal conductivity λ [W·m^{-1}·K^{-1}]. The heat transfer between metal and plastic at the boundary was assumed to be ideal. Thereby, the phase transition of thermoplastic material was considered by temperature dependent material data. It should be noted that only the melting process is represented in the model and solidification behavior was not taken into account.

$$\dot{Q} = \rho c_p \frac{\partial T}{\partial t} - \nabla(\lambda \nabla T) \quad (1)$$

Furthermore, convective cooling as well as thermal radiation were considered for heat flow density $\dot{q}$ [W·m^{-2}] into the environment which depends on the heat transfer coefficient h [W·m^{-2}·K^{-1}], the temperature of the environment

T_0 [K], the emission coefficient ε [1] and the Stefan-Boltzmann constant σ [$W \cdot m^{-2} \cdot K^{-4}$] (2).

$$\dot{q} = h(T-T_0)+\varepsilon\sigma\left(T^4-T_0^4\right) \quad (2)$$

The laser beam was modelled as heat flow density at the model boundary. Thereby, the top hat intensity distribution of the diode laser allows the abstraction as constant beam power P_L [W] over the focal diameter d_L [m]. The absorption coefficient A [1] was set constant (3). This heat flow density was applied in time interval between 0 s and joining time t_L.

$$\dot{q} = A \cdot \frac{P_L}{d_L^2} \cdot \frac{4}{\pi} \quad (3)$$

The model geometry and its boundary conditions as well as related material data are shown in figure 2. All domains are set to initial temperature T_0 [K] at process start. The mesh consists of square elements with an edge length of 0.1 mm within the area of the melting layer. In transient analysis, time steps of 0.1 s were used to investigate the time-dependent growth of the melting layer according its thickness and diameter. Due to the large overlap area of 100 x 75 mm², it was not necessary to take the clamping device into account.

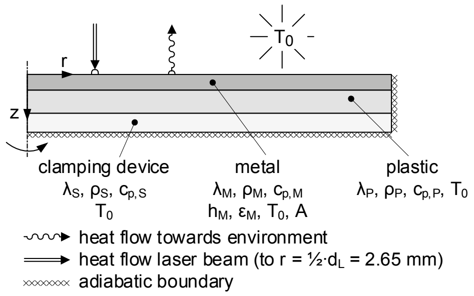

Fig. 2. Experimental setup for manufacturing hybrid joints

3.2. Sensitivity and thermal efficiency

The sensitivity of the melting layer against process parameters, the joining geometry and the material properties are investigated based on the numerical simulation. Therefore, a model material with constant material parameters was used. The selected quantities follow typical properties of technical polymers, e. g. polyamide or polypropylene (see Table 1). This method allows the specific manipulation of the material data in a wide range to gain information on the dependency of the melting layer on the material properties.

Table 1. Data of the model material for sensitivity analysis

material property	symbol	dimension	quantity
begin of melting interval	T_{im}	°C	200
end of melting interval	T_{em}	°C	230
melting enthalpy	H	$kJ \cdot kg^{-1}$	50
degradation temperature	T_d	°C	400
thermal conductivity	λ	$W \cdot m^{-1} \cdot K^{-1}$	0.25
specific heat	c_p	$J \cdot kg^{-1} \cdot K^{-1}$	1000
Density	ρ	$kg \cdot m^{-3}$	1000

Furthermore, the thermal efficiency will be investigated depending on significant process parameters. Referring to [15], the thermal efficiency is η_{th} [1] the ratio between process power Pp [W] and absorbed laser power P_A [W] (4). In contrast to the experimental investigations, the absorbed laser beam power allows a comparison between different metals on the same absorbed beam power level regardless the absorption coefficient and its influencing parameters, e. g. reflection loss.

$$\eta_{th} = \frac{P_P}{P_A} \quad (4)$$

The process power P_p is responsible for creating the melting layer with the volume V [m³] for a joining time t_L [s] in which the laser is active. Assuming that the melting layer is formed above the temperature T_{im} (as begin of thermoplastic's melting interval) and avoidance of massive thermal degradation, the process power P_p will follow (5). Based on the model material, the specific heat c_p as well as density ρ remain constant.

$$P_P = \rho \cdot V \cdot \frac{1}{t_L} \cdot \left[c_p \cdot \left(T_{im}-T_0\right)+\Delta H\right] \quad (5)$$

4. Results and discussion

4.1. Validation of the numerical simulation

The extensive validation of the numerical simulation is based on all named material combinations and parameters. Figure 4 compares the melting layer thickness between experiment (exp.) and simulation (sim.) for joints of EN AW 6082 with PA 6, PA 6.6 and PP. The correlation between joining time respectively energy input in the experiment is expressed by the numerical simulation as well. Thereby, the melting layer thickness grows over joining time and increases from PA 6.6 ($T_{im} \approx 235$ °C) over PA 6 ($T_{im} \approx 191$ °C) to PP ($T_{im} \approx 126$ °C). Consequently, the lower the melting interval the larger the melting layer thickness is.

From a quantitative point of view, the maximum deviation between simulation and experiment is about 9.9 % for PA 6.6 at a joining time of 1 s which is equivalent to 8.8 µm. This leads to a high agreement between simulation and experiment. It should be noted that there was no significant influence on the results between the surface condition as delivered and laser-structured grooves on micro-scale.

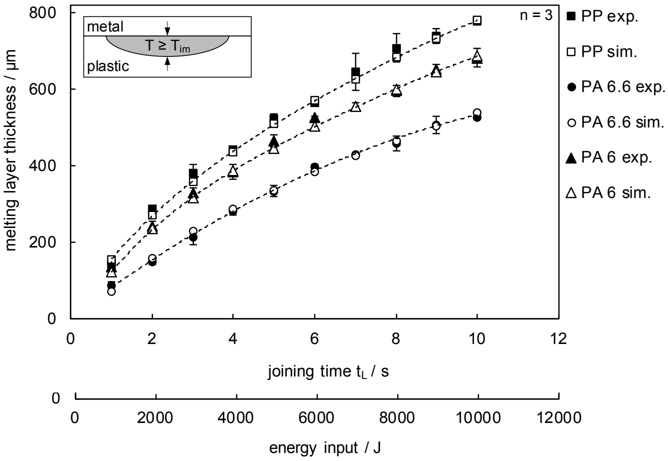

Fig. 3. Comparison between simulation and experiment regarding melting layer thickness (EN AW 6082, P_L = 1000 W)

A more detailed observation is given by a comparison between isothermal characteristic and experiment based on T_{im} as begin respectively T_{em} as end of melting interval (figure 4). The example is given for 1.4301 as metal joining partner, but aluminum shows comparable results. The geometry of the melting layer is sufficiently given by the numerical simulation and correlates well with the T_{im} isotherm. The deviation in diameter (Δ) is always higher than in melting layer thickness but also below 10 % overall investigations. This behavior is caused by the contact conditions. In the numerical simulation, the contact is idealized and constant, whereas the experiment shows a slight change in contact conditions during the joining process due to the volume increase during phase transition.

The temperature distribution over the metal thickness is relatively even for the relevant isotherms. Decomposition temperature T_d is not exceeded wherefore sporadically appearing bubbles are moisture-based. Moreover, a wide range of the melting layer is partially molten because of temperatures between T_{im} and T_{em}. In this area, solid and liquid phases occur simultaneously which results in higher viscosity and could prevent a proper surface penetration.

The temperature distribution provides precise information about the melting layer and clarifies the occurrence of a partially molten zone between isotherm T_{im} and T_{em} which was also presumed in morphological investigations [7, 10].

4.2. Sensitivity of the melting layer to process parameters

The sensitivity analysis is carried out based on the validated model, although a model material is used for varying a large number of parameters and simultaneously ensure comparability between the results.

At first, the process parameters of absorbed laser beam power P_A as well as the focal diameter d_L were investigated towards their impact on melting layer thickness. Figure 5 depicts the relationships for steel (left) and aluminum (right) as metal joining partner.

For a constant focal diameter, the melting layer thickness increases over absorbed laser beam power due to higher temperatures and a higher temperature gradient into the thermoplastic material. In contrast, larger focal diameters require more power to reach a comparable melting layer thickness for opposite effects. In all investigated cases, thermal degradation occurred from about 1,200 µm thickness onwards when decomposition temperature T_d is reached. Overall, steel and aluminum show a comparable behavior, although the heat loss in aluminum is significantly enhanced due to the decisive higher thermal conductivity.

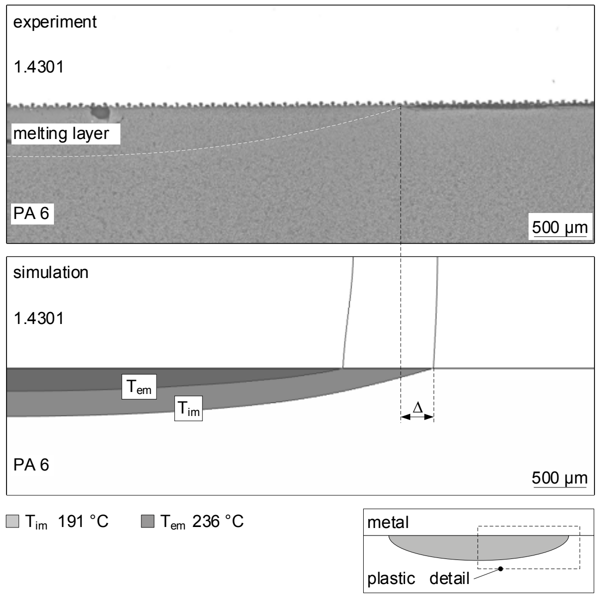

Fig. 4. Comparison between isothermal characteristics and experiment (P_L = 100 W, t_L = 5 s, 1.4301, PA 6)

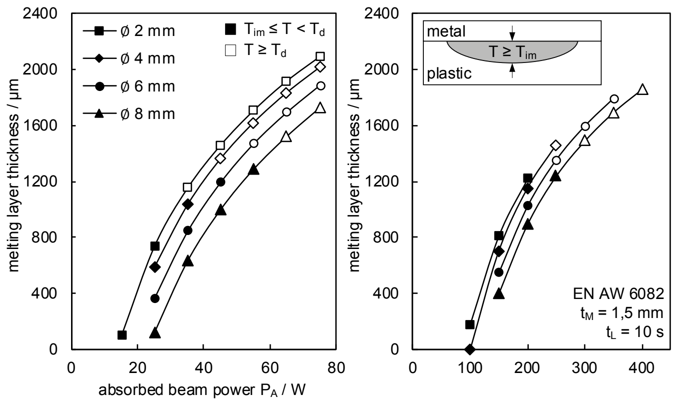

Fig. 5. Sensitivity of melting layer thickness towards absorbed beam power P_A and focal diameter d_L

It is conspicuous that the focal diameter mainly increases the maximum temperature, whereby the temperature distribution outwards is influenced subordinately. Figure 6 shows a comparison between the focal diameters 2 mm and 8 mm. Thereby, the melting layer thickness decreased significantly. Apart from that, the laser beam intensity influences the temperature distribution positively by avoiding thermal degradation of the thermoplastic and simultaneously adjusting a comparable diameter of the melting layer, which results in a comparable wetted area at the boundary layer.

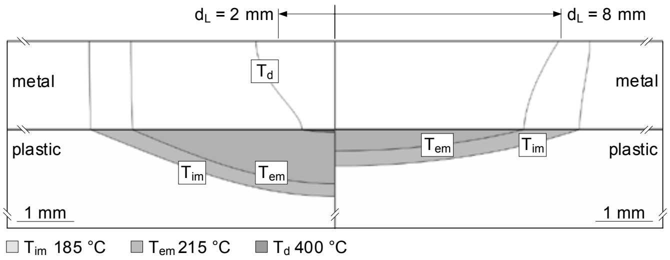

Fig. 6. Melting layer shape for focal diameter of 2 mm and 8 mm (1.4301, P_A = 35 W, t_L = 10 s, t_M = 1.5 mm)

4.3. Sensitivity of the melting layer to material properties

The model material allows a variation of the parameters thermal conductivity, density and specific heat as well as a shift of the melting interval and melting enthalpy. The adjustability of parameters provides a further understanding of their effect towards the melting layer.

Starting point is the view on thermal conductivity, density and specific heat capacity. In order to compare all three parameters, the examination is following the variables of the thermal diffusivity a [$m^2 \cdot s^{-1}$] (figure 7).

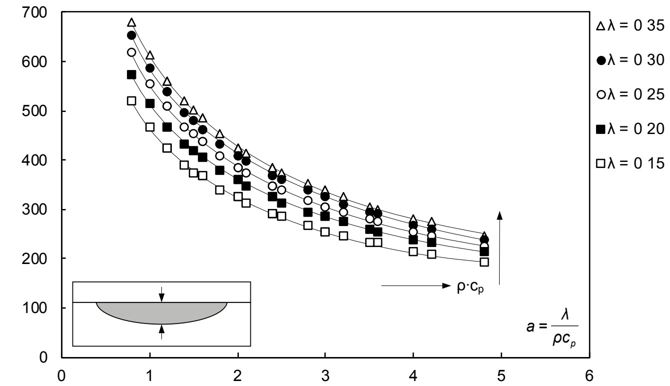

Fig. 7. Effect of thermal conductivity and volumetric heat capacity on melting layer thickness (EN AW 6082, P_L = 1000 W, t_M = 1.5 mm, t_L = 10 s)

Therefore, the thermal diffusivity a is plotted on the vertical axis and the volumetric heat capacity (density multiplied by specific heat capacity) on the horizontal axis. The resulting array of curves is caused by different thermal conductivities. Thereby, an increasing volumetric heat capacity requires a higher energy input to achieve the necessary temperatures in order to form the melting layer. In contrast, a higher thermal conductivity leads to larger melting layers due to a faster heat transfer within the plastic. For example, the increase of thermal conductivity from 0.15 $W \cdot m^{-1} \cdot K^{-1}$ up to 0.35 $W \cdot m^{-1} \cdot K^{-1}$ leads to a larger melting layer thickness between 26 % and 31 %. Thereby, the maximum temperatures are not significantly reduced (≤ 10 K). Additionally, the melting layer diameter is just slightly growing up to 12 %.

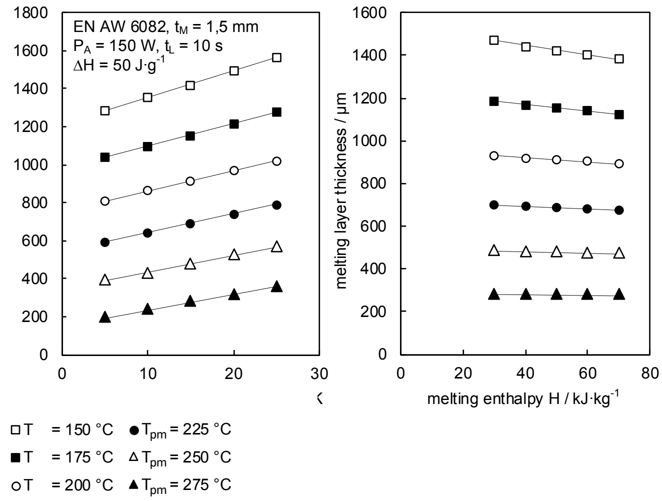

Fig. 8. Effect of melting interval width and melting enthalpy on melting layer thickness (EN AW 6082, P_L = 1000 W, t_M = 1,5 mm, t_L = 10 s)

Furthermore, the influence of the melting interval and the melting enthalpy will be examined. The melting interval is characterized by T_{im} and T_{em} and the difference between both temperatures is defined as melting interval width ΔT [K]. The model material presents a symmetrical melting interval with T_{pm} as peak temperature in the middle. The dependence of melting layer thickness on T_{pm} and ΔT is given in figure 8. As expected, the melting layer grows with decreasing peak temperatures. A broader melting interval shifts the begin of the melting interval to lower temperatures as well, why the melting layer is increasing for larger ΔT too.

In contrast, the melting enthalpy shows a minor influence on the melting layer thickness. The largest melting layer thickness results for T_{pm} = 150 °C, the difference between 30 $kJ \cdot kg^{-1}$ and 70 $kJ \cdot kg^{-1}$ is about 6 %.

4.4. Sensitivity of the melting layer to geometrical parameters

The investigations on geometrical parameters will focus on the metal sheet thickness t_M. Figure 9 shows the effect of varying t_M from 1 mm up to 4 mm. Basically, the joining process can be carried out within the considered sheet thicknesses, but higher laser beam power is required to form a melting layer up to 4 mm. The main reason is the increasing heat loss in the metal joining partner. Moreover, an increasing sheet thickness requires more time for a sufficient heat transfer into the plastic material. Analogous to the investigations on focal diameter (see 4.2), thermal degradation occurs from about 1,200 µm melting layer thickness onwards.

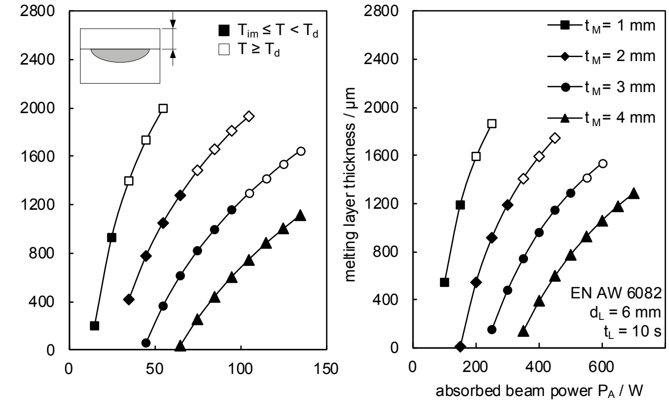

Fig. 9. Sensitivity of melting layer against the metal sheet thickness

Regarding geometry of the melting layer, figure 10 shows a comparison between a metal sheet thickness of 1 mm and 4 mm. Due to the reduced influence of the focal diameter, the adjustment of the absorbed beam power results in a comparable melting layer geometry for the depicted metal sheet thicknesses. The absorbed beam power is increased by factor 4.7. The temperature distribution is clearly shifted and the isotherm for thermal degradation T_d is reached within the 4 mm sheet but does not reach the boundary layer. This clarifies the higher heat loss within the metal joining partner.

The metal sheet thickness shows a high effect regarding the required beam power to form a joint. On this basis, the thermal efficiency will be investigated to gain information about the percentage of beam power which is actually used for creating the melting layer compared to losses with the materials respectively the environment.

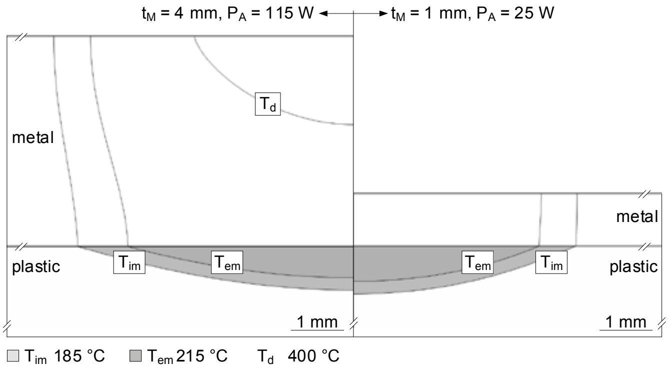

Fig. 10. Comparison between simulation and experiment regarding melting layer thickness (1.4301, d_L = 6 mm)

4.5. Thermal efficiency of the process

The thermal efficiency of the process is shown in figure 11 for 1.4301 an EN AW 6082 depending the absorbed beam power P_A and metal sheet thickness. In heat conduction joining, the beam power is absorbed by the metal sheet whereby the plastic material is heated indirectly. Hence, the heat loss is mainly influenced by the metal joining partner and its thickness. These heat losses are increasing with metal sheet thickness and result in a reduced thermal efficiency. For a sheet thickness of 1 mm, a maximum thermal efficiency of 9.8 % for 1.4301 and 5.7 % for EN AW 6082 is achieved. The difference between is led back to the different thermal conductivity of both metals. However, decomposition temperature is exceeded in these cases and would result in bubble formation. By avoiding the thermal degradation, a maximum thermal efficiency of 3 % respectively 2 % is reached. Therefore, a very small share of the absorbed beam power is used for joint formation.

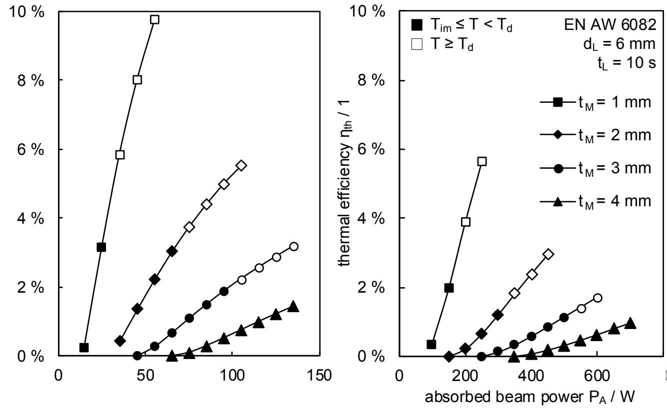

Fig. 11. Thermal efficiency for spot joints manufactured of 1.4301 and EN AW 6082 with the model material

These fundamental investigations clarify the high percentage of heat loss in thermal joining. It should be noted that the thermal efficiency considers only the absorbed laser beam power and reflection loss is not taken into account.

5. Conclusion

The melting layer in thermoplastic material is responsible for forming a joint between metals and plastics. A numerical model of heat conduction joining was validated by joints between 1.4301 and EN AW 6082 in combination with PA 6, PA 6.6 and PP. Further investigations regarding the sensitivity of the melting layer against process parameters, metal sheet thickness and material properties were based on a model material. Due to the large effect of the metal sheet thickness in heat conduction joining, the thermal efficiency was examined and illustrates the small share of absorbed beam power used for joint formation in heat conduction joining.

Further investigations will focus on the formation of line joints in overlap configuration to increase thermal efficiency by heat accumulation, material design and adjusted intensity distributions. A benchmark between contour and simultaneous joining will provide further knowledge to process design and the effect on distortion. In addition, the melting layer's effect on mechanical properties will be investigated.

References

[1] Katayama S; Kawahito Y. Laser direct joining of metal and plastic. Scripta Materialia 59, 2008, p. 1247-1250
[2] Katayama S, Kawahito Y, Niwa Y, Kubota S. Laser-assisted metal and plastic joining. Proceedings of LANE 2007, p. 41-51.
[3] Mitschang P, Velthuis R, Emrich S, Kopnarski M. Induction Heated Joining of Aluminium and Carbon Fiber Reinforced Nylon 66. Journal of Thermoplastic Composite Materials 22, 2009, p. 767-801.

[4] Heckert A, Singer C, Zaeh MF, Daub R, Zeilinger T. Gas-tight thermally joined metal-thermoplastic connections by pulsed laser surface pre-treatment. Physics Procedia 83, p. 1083-1093.
[5] Heckert A, Zaeh MF. Laser Surface Pre-treatment of Aluminium for Hybrid Joints with Glass Fibre Reinforced Thermoplastics. Journal of Laser Applications 27, 2015.
[6] Amend P, Häfner T, Gränitz M, Roth S, Schmidt M. Effect of ultrashort pulse laser structuring of stainless steel on laser-based heat conduction joining of polyamide steel hybrids. Physics Procedia 83, 2016, p. 1130-1136.
[7] Schricker K, Stambke M, Bergmann JP, Bräutigam K. Laser-Based Joining of Thermoplastics to Metals: Influence of Varied Ambient Conitions on Joint Performance and Microstructure. International Journal of Polymer Science, 2016.
[8] Roesner A, Olowinsky A, Gillner A. Long term stability of laser joined plastic metal parts. Physics Procedia 41, 2013, p. 169-171.
[9] Jung DJ, Cheon J, Na SJ. Effect of surface pre-oxidaten on laser assisted joining of acrylonitrile butadiene styrene (ABS) and zinc coated steel. Materials and Design 99, 2016, p. 1-9.
[10] Schricker K, Stambke M, Bergmann JP. Experimental invesigations and modeling of the melting layer in polymer-metal hybrid structures. Welding in the World 59, 2014, p. 407-412.
[11] Amend P, Kapfenberger C, Kölbl S, Kohl B, Roth S, Schmidt M. Experimental and simulative investigations on laser-based joining of thermoplastic metal hybrids. Proceedings of LAMP 2015, 2015.
[12] Jiao J, Wang Q, Zan S, Zhang W. Numerical and experimental investigation on joining CFRTP and stainless steel using fiber lasers. Journal of Materials Processing Technology 240, 2017, p. 362-369.
[13] Rarazila Y, Miyashita Y, Hua W, Mutoh Y, Otsuka Y. YAG Lase Spot Welding of PET and Metallic Materials. Journal of Laser Micro/Nanoengineering 6, 2011, p. 69-74.
[14] Rodriguez-Vidal E, Lambarri J, Sorriano C, Sanz C, Verhaeghe G. A combined experimental and numerical approach to the laser joining of hybrid Polymer – Metal parts. Physics Procedia 56, 2014, p. 835-844.
[15] Huegel H, Graf T. Laser in der Fertigung. 2nd ed. Springer, 2014.

This is a resupply of March 2023 as the template used in the publication of the original article contained errors. The content of the article has remained unaffected.